Atmos. Meas. Tech., 16, 547–561, 2023
https://doi.org/10.5194/amt-16-547-2023

Atmospheric Measurement Techniques
Open Access
EGU

In situ ground-based mobile measurement of lightning events above central Europe

Jakub Kákona[1,2], Jan Mikeš[1], Iva Ambrožová[2], Ondřej Ploc[2], Olena Velychko[2], Lembit Sihver[2,3], and Martin Kákona[2]

[1]Faculty of Electrical Engineering, Czech Technical University in Prague, 166 27 Prague, Czech Republic
[2]Nuclear Physics Institute of the Czech Academy of Sciences, 250 68 Řež, Czech Republic
[3]Department of Radiation Physics, Atominstitut, Technische Universität Wien, 1020 Vienna, Austria

Correspondence: Jakub Kákona (kakonjak@fel.cvut.cz)

Received: 23 May 2022 – Discussion started: 10 October 2022
Revised: 6 December 2022 – Accepted: 7 December 2022 – Published: 30 January 2023

Abstract. This article describes the equipment (and the advantages of the equipment) used for in situ ground measurements of thunderstorm phenomena with measuring cars. By using all-sky high-speed cameras, radio receivers, and electric field measurements, typical lightning discharges in the central European region have been characterized. Measurements of ionizing radiation during storms using a gamma spectrometer were also performed. At ground level, no ionizing radiation originating from storm clouds was detected, although during other experiments (using the same equipment at lower altitudes corresponding to the lower part of storm clouds) ionizing radiation was detected. We showed that radio antennas with appropriately constructed receivers and all-sky high-speed cameras are devices that can significantly contribute to the understanding of processes taking place in storm clouds during lightning discharges. On the contrary, measurements of the vertical electric field did not provide any new information about the processes occurring in thunderclouds.

1 Introduction

The activity of storms is associated with many processes, the natures of which are not yet fully understood nor clarified. This includes the process of cloud electrification and subsequent electric discharge, which is the most prominent manifestation of thunderstorms. As a result, the forecasting and prediction of storm activity and the related dangers are often very unreliable.

Storm activities are also associated with the generation of ionizing radiation. It is believed that this radiation is bremsstrahlung ("deceleration radiation") generated by electrons accelerated by an electric field in thunderclouds. The electrons that are accelerated to relativistic velocities are called relativistic runaway electron avalanches (RREAs), and these RREAs then interact with the atoms in the atmosphere (Dwyer, 2003; Gurevich et al., 1992). This causes a phenomenon that is often inaccurately called terrestrial gamma-ray flash (TGF) (Fishman et al., 1994) or other phenomena like thunderstorm ground enhancement (TGE) (Chilingarian, 2013; Torii et al., 2002). Furthermore, experimental results have shown that other ionizing radiation manifestations generated by storms exist. For example, there has been experimental evidence of the interaction of high-energy photons with the atmosphere causing nuclear reactions (Enoto et al., 2017). The ionizing radiation that is thought to be associated with storm activity has been measured using satellites in orbit around the Earth (e.g., Østgaard et al., 2019), using aircraft flying inside or in the vicinity of storm clouds (Chilingarian et al., 2011; Kochkin et al., 2017; McCarthy and Parks, 1985; Parks et al., 1981), or using high-mountain observatories e.g., (Chum et al., 2020; Tsuchiya et al., 2009). Currently, there are only a few measurements that could confirm the existence of ionizing radiation at lower altitudes; however, special storms that occur in the winter season in Japan, during which storm clouds emerge low above the ground, are an exception (Michimoto, 2007).

One of the most interesting measurements performed to date has been the mapping of a radio signal emitted by

lightning (Rison et al., 1999; Wu et al., 2018). TGF observations utilizing ground detectors with simultaneous lightning mapping using radio signals exist (Abbasi et al., 2018). Despite these very detailed observations, the exact location of the source of the ionizing radiation within the storm cloud remains unknown (Belz et al., 2020). Moreover, TGFs have only rarely successfully been measured at ground level (Kereszy et al., 2022; Rakov and Kereszy, 2022; Dwyer et al., 2012; Wada et al., 2019).

To be able to measure the different processes that occur during thunderstorms, we equipped cars with measuring equipment. These cars are able to move to locations with predicted storm activity and, thus, react to specific storm developments and perform ground measurements directly at the storm site.

During the 2021 summer storm season, we carried out many expeditions in the Czech Republic and Slovakia using the equipment described in detail below. This allowed us to measure the electrostatic, magnetic, electromagnetic, and optical properties of storms, including ionizing radiation. In this paper, we present the results of these measurements and outline how we characterized the recorded lightning events, especially their duration. We relate optical observations to measurements of electromagnetic radiation in the radio spectrum and to changes in the electric and magnetic fields at the measuring site. Via the comparison of different obtained lightning records with each other, we are able to reconstruct the individual phases of the lighting events in the optical spectrum.

Figure 1. The CAR0 measuring car with the instruments mounted on the roof platform.

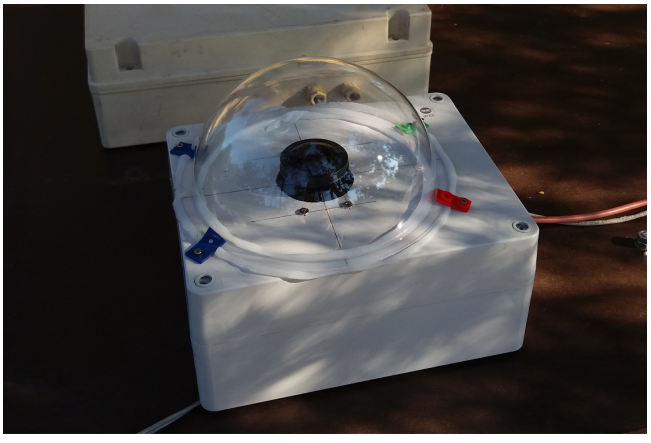

Figure 2. Camera with a wide-angle CS camera lens and equipped with an infrared-blocking filter mounted in front of the LUX1310 CMOS sensor.

2 Measuring equipment

In order to determine the necessary parameters of lightning activity (lightning events' timestamps, lightning type, and location), we equipped two measuring cars, CAR0 and CAR1, with high-speed all-sky cameras and radio receivers (see Fig. 1). The cars were used to transport and power the instruments in the proximity of thunderstorms. The car cabin also served as partial protection for instrument operators.

2.1 High-speed all-sky cameras

A Chronos 1.4 (CR14-1.0-16M) camera (KronTechInc., 2021) was mounted in a waterproof SolidBox 69200. The box was covered with a plexiglass dome, 200 mm Duradom as per the manufacturer's designation, and is depicted in Fig. 2.

The video resolution of the camera is 928 pixels × 928 pixels with 1612.33 frames per second and a constant shutter speed from 4.9 to 34 µs during daytime thunderstorms and a maximal shutter speed of 614.6 µs during nighttime thunderstorms. The shutter speed is set by the instrument operator depending on current weather conditions. The video length saved by the camera was set to 2 or 3 s. The format of the videos saved was H.264, resulting in MPEG-4 (.mp4) video, which sacrifices some quality for better compression. The main possible loss is gamma-encoded brightness, which possibly alters the absolute values of the real brightness of recorded lightning.

The camera lenses that we used were FE185C057HA-1 (Fujifilm, 2021). Therefore, the high-speed camera was only sensitive to visible light. This spectral baseband was selected to minimize the absorption of light generated by lightning in the atmosphere.

2.2 Radio frequency receivers

Different radio frequency receivers were used to record the radio emissions generated by lightning activities. The main objective was to cover a wide radio frequency band. The very low frequency (VLF) radio frequency band is known to be sensitive mainly to large (size) and high-current lightning channels, such as the return stroke. On the contrary, the

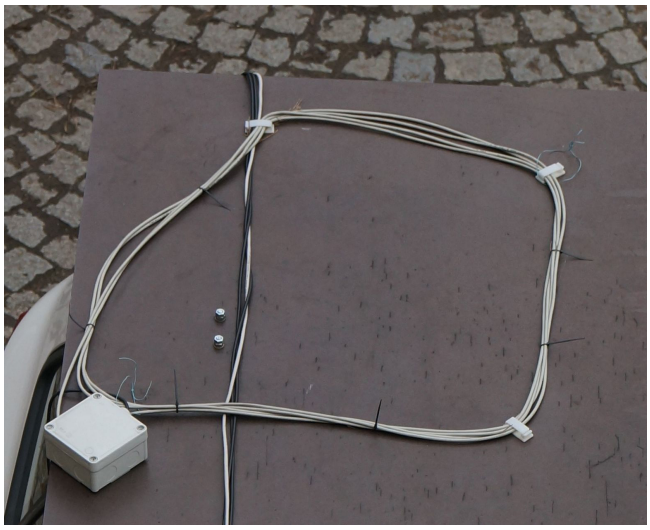

Figure 3. The STP loop antenna, mounted on the CAR1, has a resonant frequency of 100 kHz. Its signal was directly sampled by an oscilloscope placed inside the car.

ultrahigh-frequency (UHF) radio frequency band involves radiation almost exclusively associated with the fine structure of lightning (Shi et al., 2019).

2.2.1 VLF signal receiver

The VLF signal receiver is based on a magnetic loop antenna and storage oscilloscope with a control computer for the data readout. For one lightning event, we could record 800 ms of 8 bit samples with a sampling rate of 250 MS s^{-1} (mega samples per second).

The antenna design was based on the use of the VLFANT01 (MLAB, 2017) module, with the 10 m shielded twisted-pair (STP) cable coiled into four loops (STP antenna). The STP antenna loop was placed horizontally directly on the plywood base mounted on the car roof (see Fig. 3 for details).

This VLF receiver system was also used for the detection of lightning and for triggering other instruments in the cars. The detection of lightning was based on the pulse width and the signal level; both parameters were set by the operator during the thunderstorm event. The range of these parameters is usually 5 to 20 µs for the pulse width and 10 to 30 mV for the signal level. An example of the measured signal can be seen in Sect. 4.3.

2.2.2 UHF signal receiver

The UHF receiver operates approximately in the 370–406 MHz band, although the exact tuning depends on the local noise within the 10 MHz receiver bandwidth. The signal is received by an array of four quadrifilar helicoidal (QFH) antennas mounted in a square-like configuration on the roof

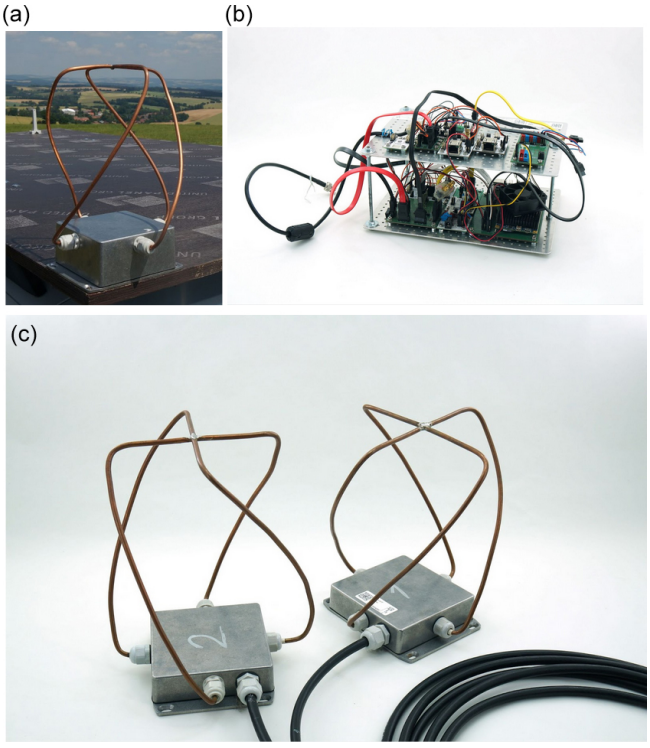

Figure 4. The platform of a QFH receiver antenna is shown in panel **(a)**. Detailed pictures of the antenna can be seen in panel **(c)**, and the receiver is shown in panel **(b)**.

platform of the measuring car, as shown in Figs. 1 and 4. The signal from each antenna is directly down-converted by a radio frequency mixer to I (in-phase) and Q (quadrature signal) analog channels. Each channel is sampled by a 12 bit analog-to-digital converter at 10 MS s^{-1}.

The construction of the receiver itself is designed in a way that enables a phase processing of the signal from the antenna array with the aim of detailed mapping of the discharge (UST, 2021). However, in the case of this experiment, only the scalar envelope of the radio signal is considered. A block diagram of the receiver is shown Fig. A1 in Appendix A.

The radio receiver, in the case of an external trigger, records a section of the configurable length of pre-trigger and post-trigger blocks which are up to 1.45 s long. The radio signal is simultaneously sampled from the whole antenna array. This feature is achieved using a ring buffer that stores the samples before the trigger. Due to a pulse-per-second (PPS) signal from an external Global Navigation Satellite System (GNSS) receiver, the resulting recorded file at the same time contains the sub-microsecond absolute time of each recorded sample.

The antennas are mounted on an electrically nonconductive, 18 mm thick plywood board (identical to CAR 1 with a VLF receiver) that is attached to the roof of the measuring car by crossbars, located above the car's metal roof.

The construction of a single antenna array element is based on the QFH design. The antenna contains two loops that are joined together on one side and connected to the active analog fronted printed circuit board (PCB) of the antenna (QFHMIX01) on the other side. The QFHMIX01 PCB is mounted in a metal enclosure. The antenna half-loops pass through the enclosure wall via waterproof cable glands. Each joint of the half-loop and QFHMIX01 PCB is considered a 40 Ω port. The signal on each port has a 90° signal phase shift in relation to the next port. This feature allows the processing of the signal from the antenna as quadrature I/Q data, which significantly increases the capabilities of subsequent signal processing.

2.3 Ionizing radiation detectors

During the whole measuring campaign, NaI(Tl) ionizing radiation detector sensors and a silicon photomultipliers (SiPM) were used. Details of the AIRDOS-C gamma spectrometer used can be found in Velychko et al. (2022). The energy deposition range of this device is 200 keV to 40 MeV. The time resolution between two incident ionizing radiation events is 100 µs for particles with deposited energy above 1 MeV. For lower energies, only a 15 s integration of events is provided. The NaI(Tl) crystal with the SiPM and preamplifier is shielded in a metallic box.

2.4 Electric field mill

The electric field is measured using the Kleinwächter EFM 115 electric field mill (EFM) from which the analog signal output leads directly to the data logger that contains a GPS receiver for timestamping the record (MLAB, 2021). The logging time resolution is 110 ms.

2.5 Meteorological instruments

In order to determine the meteorological situation in the vicinity of the cars during the measurement, the cars were equipped with several meteorological sensors: a distrometer (UST, 2020), an anemometer (MLAB, 2020), and a thermometer with a barometer (MLAB, 2015).

3 Observational methods

Observations were carried out using a gradually improved strategy with the aim of getting the measuring cars (especially the car equipped with radiation detectors) as close to the storm center as possible. The position of the storm center was monitored using data from the Windy (Windy, 2021) and Blitzortung.org (Wanke, 2011) third-party networks.

The measuring cars were stationary during thunderstorm measurements. Moreover, in the case of the radiation detectors, an extended static position time interval was used before and after storm activity in order to record the entire development of radiation change, including the local radiation background parameters.

During the measurement campaigns, the data recording method was developed. During the first campaigns, we were trying to make automatic recordings based on observed electromagnetic signals. This system, however, had a lot of imperfections that ultimately led to the system's abandonment in measuring car CAR0, where it was replaced by the manual activation of recording (see Fig. 5). The manual activation of recording was based on the visual perception of the operator (the observation of lightning activity). In contrast to CAR0, CAR1 maintained a semi-automatic method of activating the recording in order to compare the efficiency of both trigger methods. Thus, CAR1 had a recording trigger based on using a loop antenna and oscilloscope which generated triggers for other devices based on amplitude measurements and a length of voltage pulse on antenna output (see Fig. 6). The trigger signal was distributed via the Ethernet network, which was a solution common to both measuring cars.

During the observation itself, a significant problem was caused by the time needed to record the data measured by individual detectors; this resulted from the time period needed to store the recording from the operational memory of the devices. We were able to reduce the time, mainly by optimizing the camera settings and using different firmware. Nevertheless, the total dead time was still about 90 s for storms occurring during the day. In the case of night storms, the dead time decreased to approximately 60 s due to the image compression used. As a consequence, all lightning events were not recorded for any storm event.

4 Results

4.1 Ionizing radiation measurements

Figure 7 shows an example of ionizing radiation measurements using the AIRDOS-C gamma spectrometer. In Fig. 7a, a storm approaching a parked measuring car is displayed using data from the Blitzortung.org network. The vertical red lines mark the times when lightning was registered by the STP antenna. Figure 7b shows the number of particles registered by the ionizing radiation detector every 15 s. In this particular example, the lightning activity ceased just after 20:30 UTC. The graph shows an approximate 30 % increase in the ionizing radiation flux. This increase is related to a radon progenies washout from the atmosphere caused by rain that started at 19:45 UTC.

Figure 8 shows a short time period of ionizing radiation measurement at the time when the storm was closest to the car. Individual particles of ionizing radiation registered versus detected lightning are shown. Only particles that have passed on energies higher than 2.4 MeV to the detector are displayed.

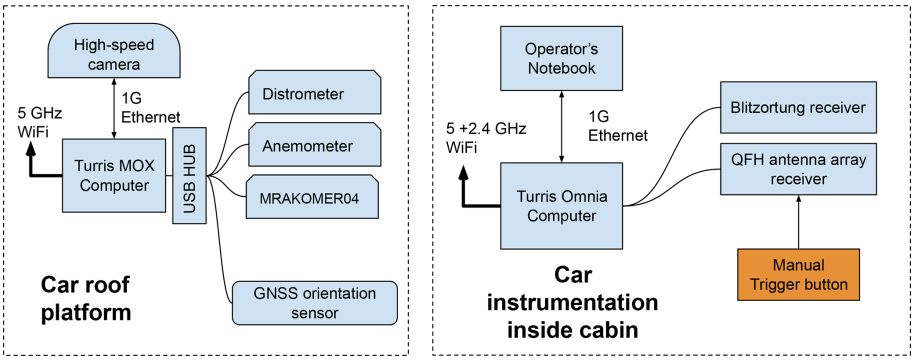

Figure 5. CRREAT (Research Center of Cosmic Rays and Radiation Events in the Atmosphere) CAR0 instrumentation schematic diagram.

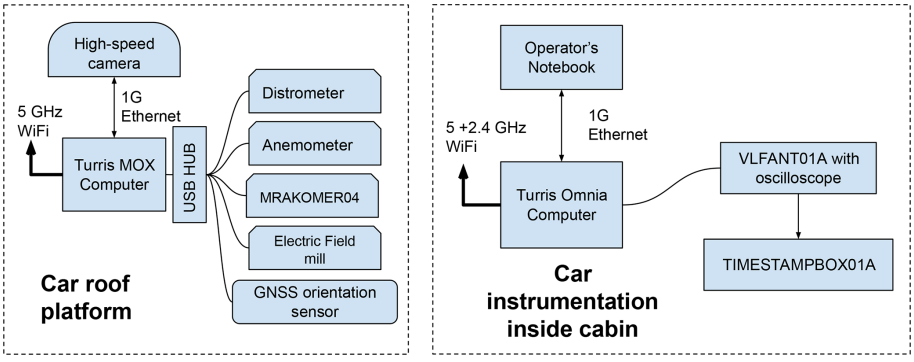

Figure 6. CRREAT (Research Center of Cosmic Rays and Radiation Events in the Atmosphere) CAR1 instrumentation schematic diagram.

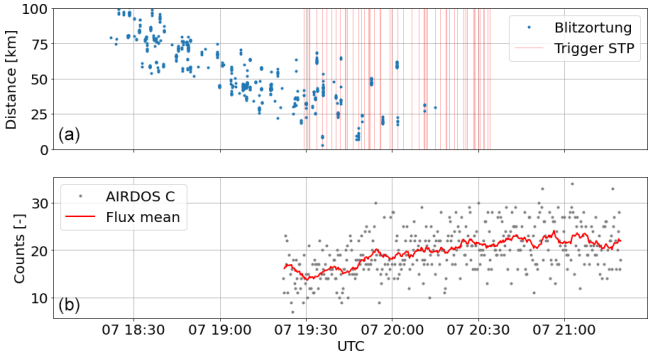

Figure 7. Measurements of ionizing radiation using a car compared with lightning registered by antennas. The beginning of the measurements using the AIRDOS-C and STP antennas corresponded to switching on the devices after parking the car at a measurement location at 19:15 UTC. The end of the measurements at 21:25 UTC corresponded to switching off the devices and leaving the measurement location.

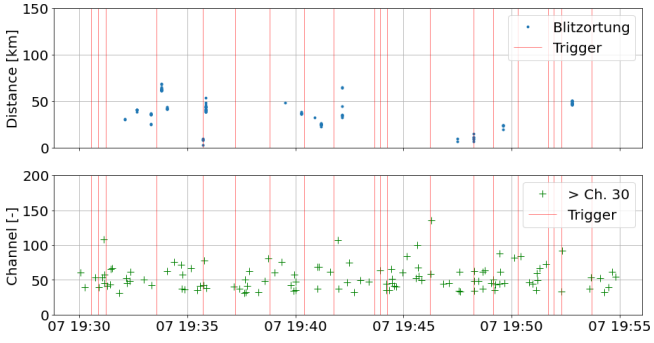

Figure 8. Lightning detected by Blitzortung.org and triggers from the STP antenna plotted together with individually registered particles of ionizing radiation above channel 30 of the gamma spectrometer.

4.2 Camera measurements

During the measurement, the camera is pointed toward the zenith and its lens allows it to capture the entire sky from horizon to horizon. For the illustration of the camera view, a plain camera frame is shown in Fig. 9. Because lightning discharges often happen inside clouds and lightning channels are not directly visible, we converted the videos of the recorded lightning to luminosity in time. The integral values of the illuminations were calculated using a script from the video recordings of the high-speed cameras. The calculations were carried out over the entire image area by summing up the values of all pixels on each image. We call these luminosity curves. The results can be seen on the graphs in Fig. 11 that depict the course of light flux over time.

Figure 9. A still-image example from the all-sky camera showing the horizon and the fish-eye lens distortion.

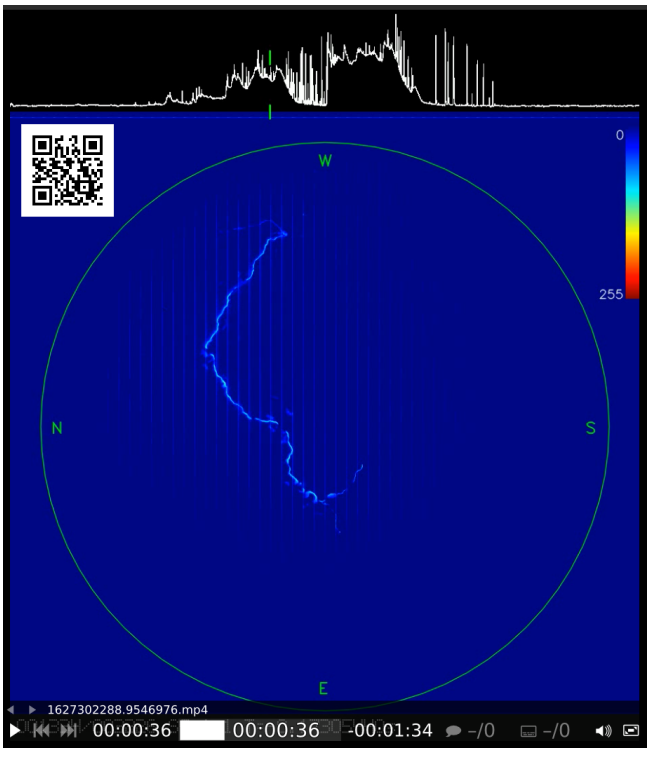

Figure 10. The reader is advised to use the inset QR code or the following link to run the video: https://doi.org/10.5446/60389 (Kakona, 2022a).

To maintain clarity, luminosity curves were added to videos, which were converted from black-and-white (BW) recordings captured by cameras to false colors in order to make the details of the lightning (that have high luminosity dynamics) visible.

Figure 10 captures one frame from a video (https://doi.org/10.5446/60389, Kakona, 2022a) that clearly shows a flash of lightning as well as the leaders and recoil leaders. During the thunderstorm recording, the camera gain was decreased in order to capture lightning that has high brightness dynamics. As a result, lightning is not visible in the video at the same time as details of clouds and surrounding terrain. The processed video has the position of the horizon marked with a green circle with an inscribed designation of the cardinal directions. In the upper part of the video, there is a white graph showing the luminosity curve with a green pointer marking the position of the current frame over time. On the right, a color palette is visible that corresponds to the brightness recorded by each camera pixel with a depth of 8 bits. The bottom line shows the number of the current frame over the total number of frames recorded, $\mathrm{Sg} = 1/1$ (information on which part of the camera's internal memory was used for recording), and the time of the current frame "$T =$" in seconds relative to the trigger.

The resulting luminosity curves contain similar parts (sharp peaks or slow changes in luminosity). Thus, we can compare the video recordings of luminosity curves with a similar progression, and we can choose those parts from several recordings that have similar luminosity curves and a visible lightning channel (not covered by clouds). This process helps us to see what lightning really looks like.

4.3 Antenna measurements

One of the advantages of measuring lightning using magnetic loop antennas is that the observation is not disturbed by optically nontransparent clouds or, as is the case for storms occurring during the day, sunlight scattered in the atmosphere. On the other hand, when we use a coil to measure the magnetic component of the electric field, we only see its changes in time or specifically a change in the current that flows through the lightning channel. If a constant current flows through the lightning channel, it is not possible to detect it using a magnetic loop antenna. Figure 12 shows an example of lightning recorded by an STP antenna and a camera at the same time. In the camera recording, a change in light conditions is clearly visible. The sky was brighter before the lightning than after it occurred. Slow changes in brightness, and thus slow changes in current, are not visible on the antenna recording. On the other hand, we see clusters of fast pulses that can give information about the development of lightning channels, which are not visible on the camera recordings because they are probably obscured by light emanated by a constant current in the main channel. Pulses that are visible on both camera and antenna recordings are recoil leaders.

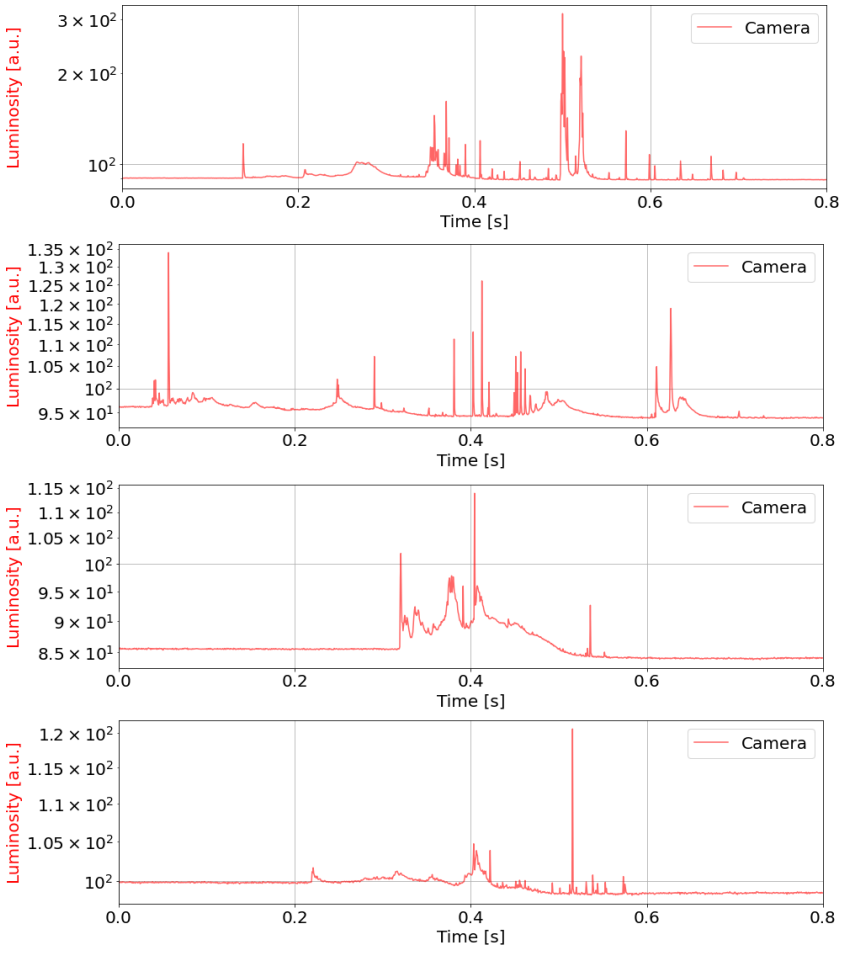

Figure 11. An example of luminosity curves for a few lightning events.

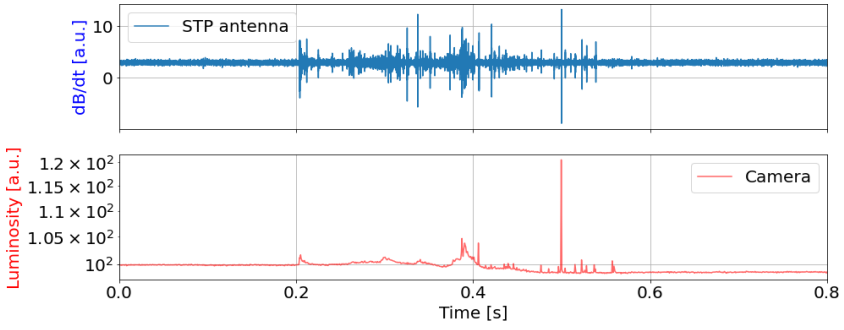

Figure 12. An example of data from the STP antenna and a comparison with camera data.

The most prominent pulse is the CG (cloud-to-ground) return stroke.

4.4 Correlation of measured lightning with a lightning detection network

We have tried to compare the detection of lightning using the STP antenna with its detection using the Blitzortung.org network. First, we have to note that not every lightning event detected by the STP antenna was recorded, as it takes several minutes to store lightning data from the oscilloscope to the data storage device. Second, not every lightning event detected by the STP antenna was detected by the Blitzortung.org network. Figure 13 shows that the STP antenna detected lightning at a different time or at a distance of more than 120 km away when the storm was closest to the car according to the Blitzortung.org network. On the contrary, as

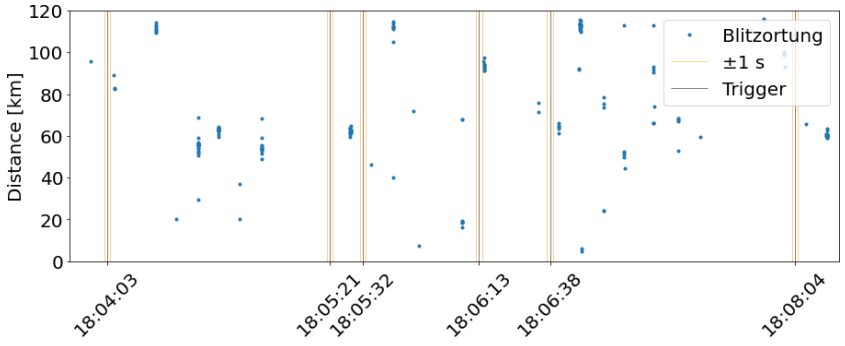

Figure 13. Correlation with "close" (less than 20 km) lightning detection.

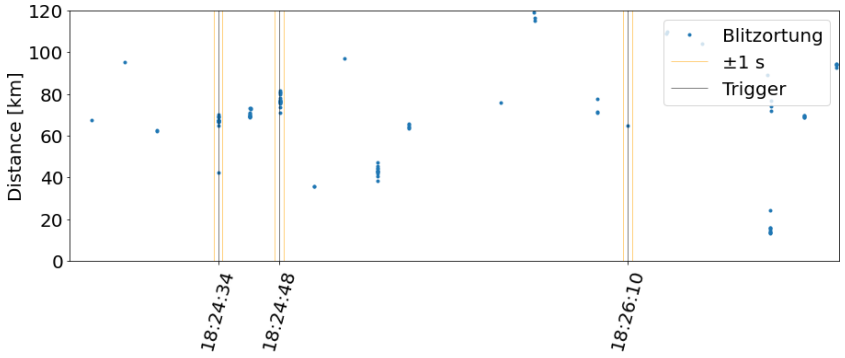

Figure 14. Correlation with "distant" (more than 40 km) lightning detection.

shown in Fig. 14, when the storm was located tens of kilometers from the observation site according to the Blitzortung.org network, we see perfect conformity with the data from the STP antenna. In both figures, an interval of ±1 s is marked around the vertical lines corresponding to the detection times.

Lightning at 18:24:48 UTC was detected by a high-speed camera (see video, https://doi.org/10.5446/60389, Kakona, 2022a). According to the video, one of the lightning channels occurred almost directly above the measurement car, but the nearest lightning event detected by Blitzortung.org was at least 70 km away. The positioning accuracy of the Blitzortung.org network is in the order of kilometers. Blitzorting.org detected discharges at a distance of 70–80 km simultaneously. Thus, we can deduce that this lightning event was more than 80 km long or that a synchronous discharge occurred 80 km away.

4.5 Electric field measurements

Figures 15 and 16 show a comparison of the vertical electric field measurements at the car measurement site with those from the camera recordings. The EFM on the car is not grounded; thus, it measures the gradient of the electric potential between the sensor and the car body. As can be seen in Fig. 15, the electric discharges occur at times of large electric field changes. However, if we look at the details of some discharges recorded by the camera (Fig. 16), we can see that the changes in the electric field do not correspond directly to individual discharges. Please note that EFM measures the vertical component of the electric field, which gives the integrated value over a large area of clouds, and the field is also deformed by the presence of a car.

5 Discussion

5.1 Lightning duration

We attempted to determine the duration of lightning events by searching for local maxima in the illumination of the camera chip in time from peaks that have a prominence higher than 2 times that of noise. Then the first and last maxima were used for the determination of the first and last snap, and the lightning duration was calculated from the frame rate. First, 10 snaps of the camera record were omitted due to possible artifacts stemming from the video data compression. The amplitude of noise was established from the first 100 frames (from frame 10 to frame 110). Examples of how we determined the duration of some lightning events are shown in Figs. 17 and 18. The histogram of the duration of lightning events is shown in Fig. 19. This histogram comprises 107 lightning events measured during 12 thunderstorms.

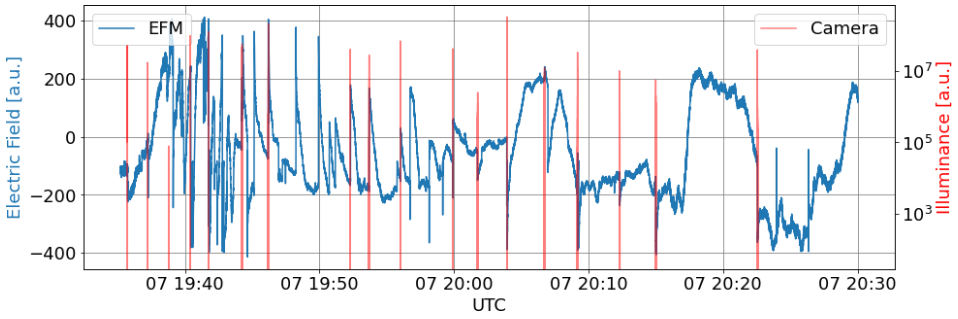

Figure 15. An example of measurements with the EFM compared with records of lightning captured on the camera.

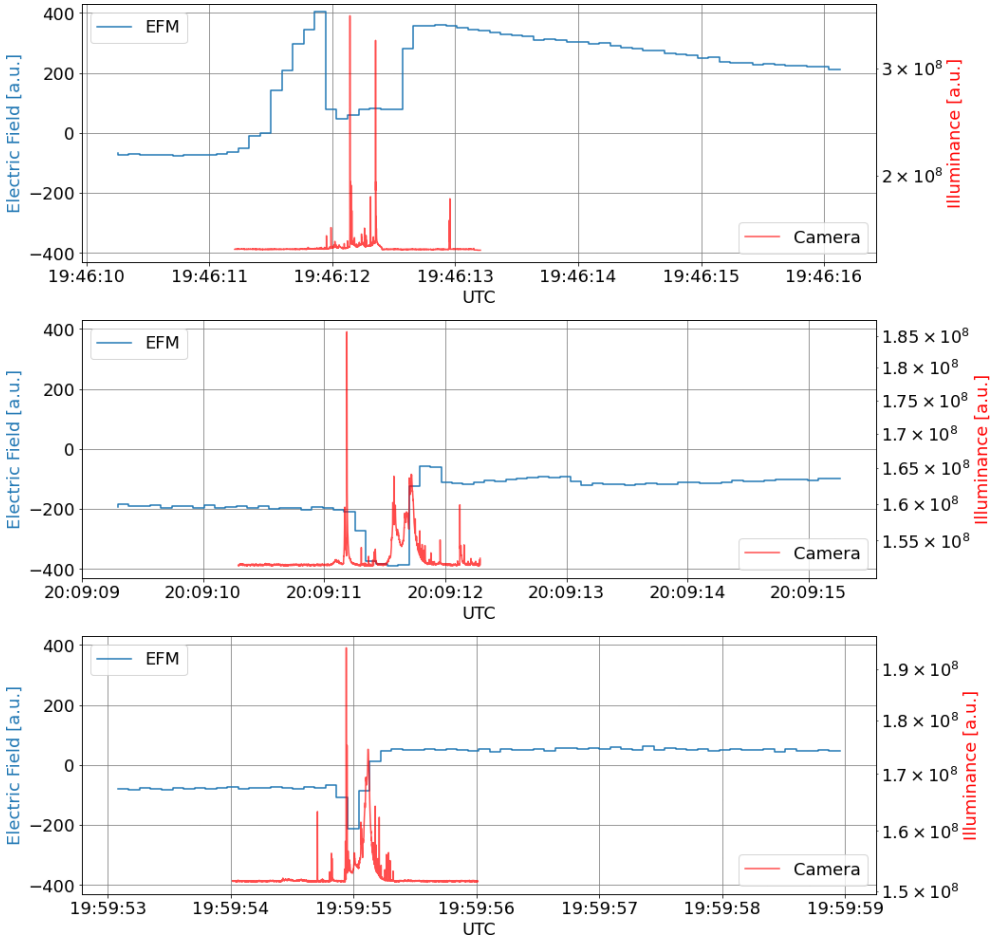

Figure 16. Details of the EFM data compared with camera data.

To calculate the total length of a lightning event from the radio signal shown in Fig. 18, we used a methodology that treats signals greater than 4σ variance, calculated from the moving window of 10 ms, as the start of the lightning discharge. This algorithm is applied symmetrically from both ends of the recorded signal. Therefore, the recording of the length of the lightning begins at the first sample of the detected signal and ends at the last sample of the recorded signal.

The measured durations are usually in the order of hundreds of milliseconds, with shorter lightning events being rare. The median duration of lightning events is 524 ms. This result is significantly longer than values reported previous studies: 200–300 ms (Rakov and Uman, 2003) and 350 ms (López et al., 2017).

The processing of lightning recordings differs for day and night storm observations, as they require different high-speed camera settings. In particular, the shutter speed (exposition

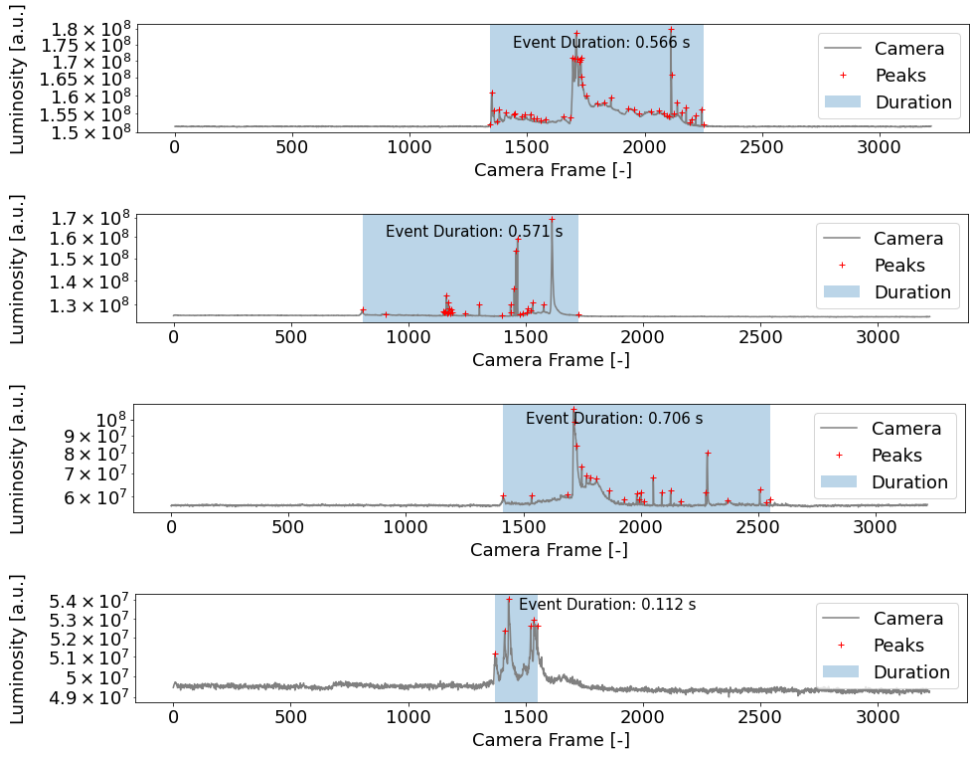

Figure 17. Examples of the detection of lightning event duration. Red crosses are detected peaks in signals generated by lightning processes. The determined length of the lightning duration is highlighted. The duration of the camera frame is 620 µs.

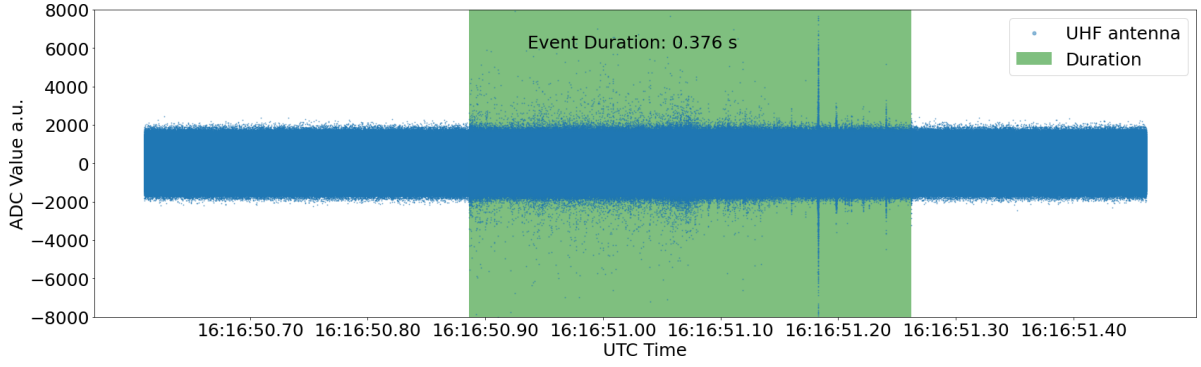

Figure 18. An example of lightning duration measurements based on radio signals captured by the UHF receiver. The length of the lightning duration is marked by the green overlay.

time) and the analog gain settings vary. This difference could affect the exact measurements of the total length of a discharge, resulting in a shortening of the estimated duration. As sunlight is scattered in the atmosphere during the daytime, weak discharges might have been omitted. Therefore, the extracted durations of lightning events could be underestimated.

From the following analysis of the lightning duration, we excluded two thunderstorms during which it was not possible to distinguish between individual lightning events (events for which there was less than 500 ms between the individual detected discharges). We considered lightning to be an "event" when the time between the individual discharges did not exceed 100 ms.

5.2 Lightning development/characterization

Data from the cameras reveal similar phases of lightning development. We provide examples of video recordings with the individual phases clearly visible and unobscured by clouds.

Figure 20 captures one frame from a video (https://doi.org/10.5446/60390, Kakona, 2022b) that shows (from $T =$

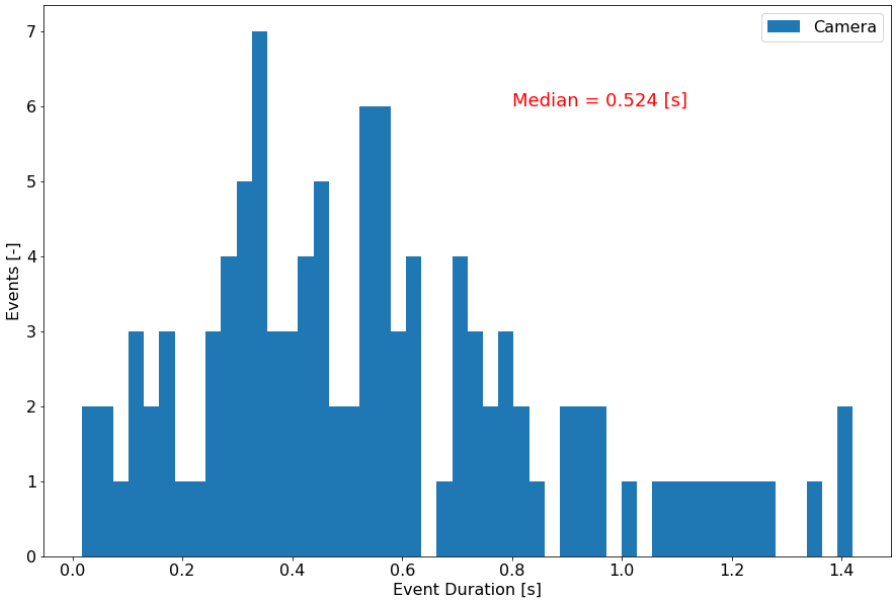

Figure 19. A histogram of the observed duration of lightning events. The histogram is based on data captured by the high-speed cameras.

+0.27 s to $T = +0.40$ s; https://av.tib.eu/media/60390#t=1:11,1:22, last access: 1 January 2023) the positive side of a leader. When the current flowing through the leader begins to weaken, recoil leaders start to appear at its end ($T = +0.38$ s; https://av.tib.eu/media/60390#t=1:21,1:30, last access: 1 January 2023). The term "recoil leader" was taken from the literature (Mazur et al., 2013). Based on our observations, however, we cannot confirm that all the visible recoil leaders reuse a pre-established ionized channel.

Figure 21 captures one frame from a video (https://doi.org/10.5446/60388, Kakona, 2022c) that shows an invisible positive leader, but only blurred recoil leaders are visible. From $T = +0.07$ s (https://av.tib.eu/media/60388#t=1:36,1:44, last access: 1 January 2023), a negative side of a leader is visible. The negative leader branches abundantly, and its propagation is faster than the positive leader and contains hot luminous ends. The second visible negative leader starts at $T = +0.25$ s (https://av.tib.eu/media/60388#t=1:51,1:59, last access: 1 January 2023). The negative leaders do not generate recoil leaders.

Based on the recordings, in which some parts of the lightning are clearly visible, we can characterize other lightning events. In Fig. 12, an example of the luminosity curve and antenna data is shown. At the very beginning, the lightning usually starts with a faint peak with a fast-rising edge (at the time 0.2 s). Then there is an optically dark phase with low luminosity. However, this quiet period is not really quiet in the radio signal; it is a phase in which a leader develops. As the leader in the cloud connects to more and more charged regions, it becomes brighter (sometimes slowly, sometimes abruptly). During and after a decrease in the current in the positive leader, the recoil leaders appear (after 0.4 s). Some

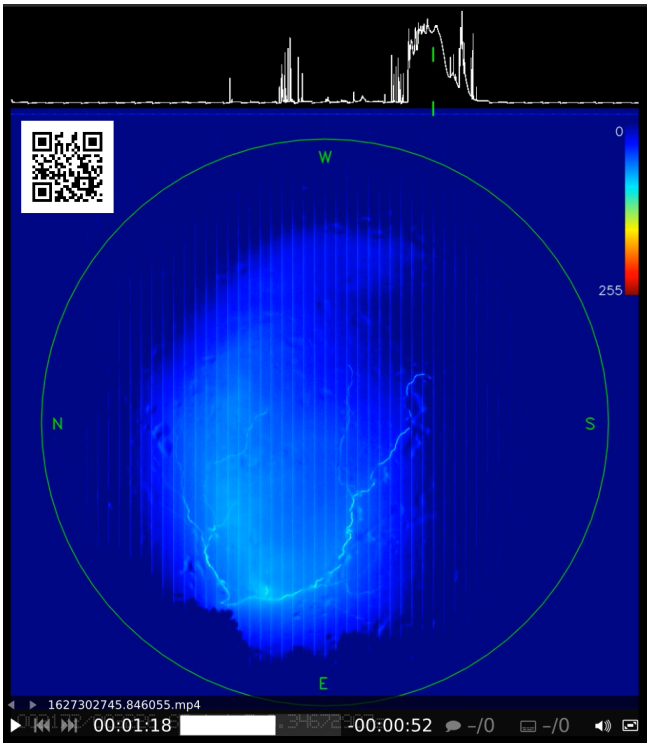

Figure 20. The reader is advised to use the inset QR code or the following link to run the video: https://doi.org/10.5446/60390 (Kakona, 2022b).

recoil leaders have high luminosity when they connect to the main channel. In the radio spectrum, we simultaneously observe peaks that correspond to short intense brightenings. In

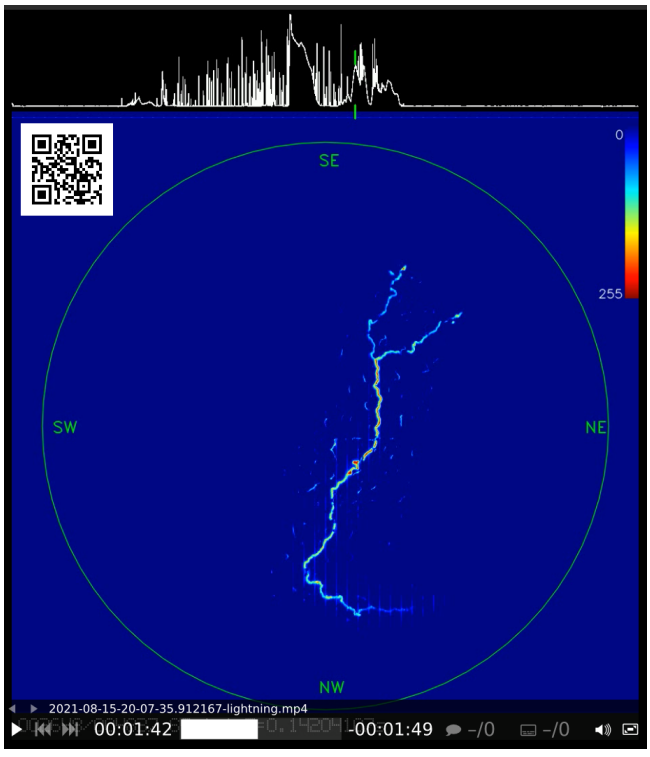

Figure 21. The reader is advised to use the inset QR code or the following link to run the video: https://doi.org/10.5446/60388 (Kakona, 2022c).

some cases the lightning results in CG discharge, which is accompanied by a high-intensity flash (at 0.5 s). However, this phenomenon does not occur very often. Using the described equipment, we registered CG return strokes in less than 10 % of cases.

6 Conclusions

During the 2021 summer storm season, we collected data on more than 100 lightning events using cars equipped with all-sky high-speed cameras, radio receivers, and electric field detectors. We conclude, based on these measurements, that the data from all-sky high-speed cameras and magnetic or electromagnetic antennas give comparable results in terms of lightning duration. The median duration of the measured lightning was 0.52 s, which is longer than values reported in the literature. We have shown that the data obtained by EFM (measurement of the vertical electric field) do not provide any new information about the development of lightning. We were also not able to prove a direct connection between the increase in ionizing radiation and lightning in the lowlands of central Europe. During further experiments, we want to focus on the triangulation of discharges, using antennas and cameras simultaneously, so that the actual dimensions of lightning and the distance from lightning can be determined. We also wish to concentrate on measuring the electric field in the horizontal plane at the altitude of the thundercloud base. We believe that these measurements could contribute to a better understanding of where and when the ionizing radiation originates during thunderstorms.

Appendix A

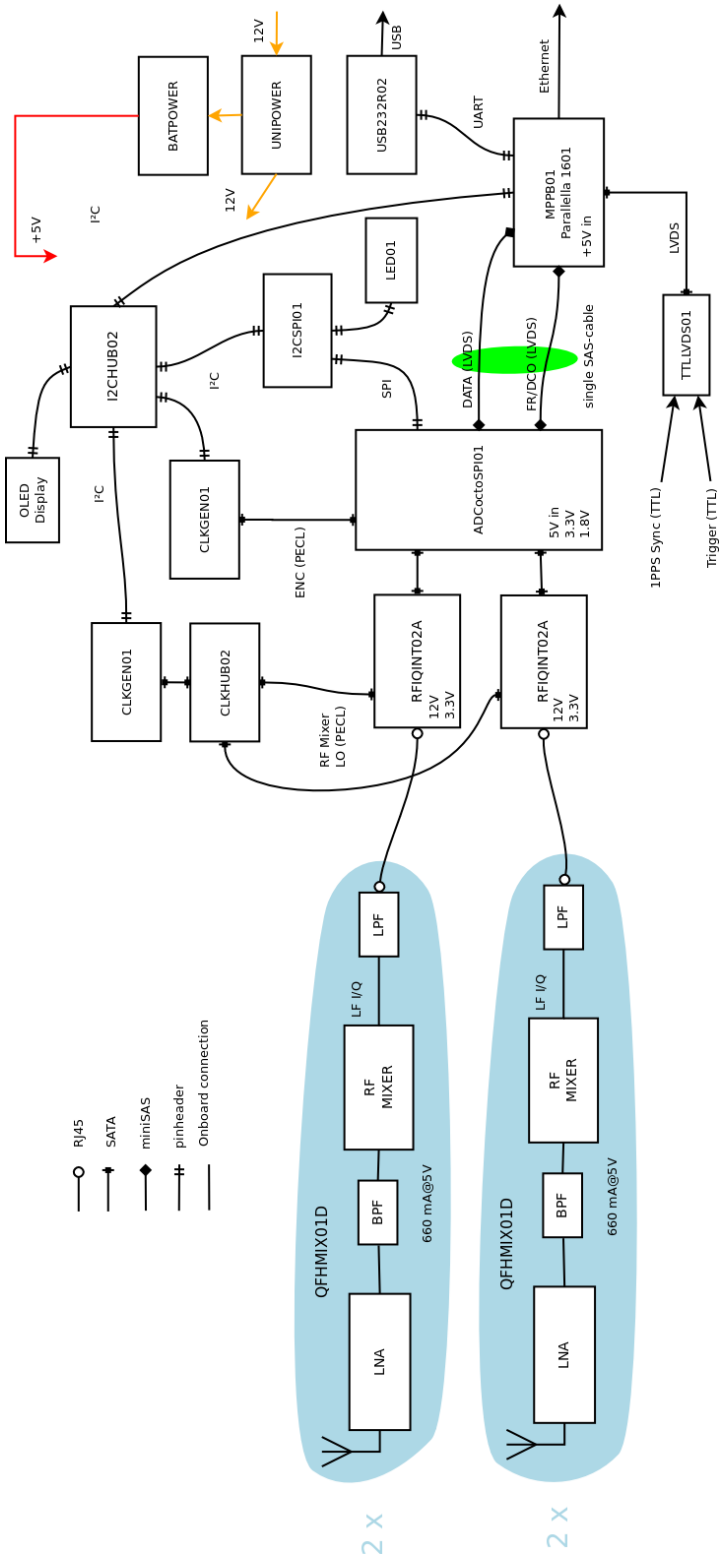

Figure A1. Block diagram of the UHF radio receiver used in the experiment. The internals of the active antenna mounted on the car roof are depicted using the blue bubbles on the left.

Data availability. All raw data can be provided by the corresponding author upon request.

Video supplement. The videos are available at TIB: https://doi.org/10.5446/60389 (Kakona, 2022a), https://doi.org/10.5446/60390 (Kakona, 2022b), and https://doi.org/10.5446/60388 (Kakona, 2022c).

Author contributions. JK and MK planned the campaign and performed the measurements. MK, JK, and OV analyzed the data. MK and JK wrote the manuscript draft, and IA, OP, LS, and JM reviewed and edited the manuscript.

Competing interests. The contact author has declared that none of the authors has any competing interests.

Disclaimer. Publisher's note: Copernicus Publications remains neutral with regard to jurisdictional claims in published maps and institutional affiliations.

Acknowledgements. This work was supported by EU Operational Program Research, Development, and Education within the framework of the CRREAT (Research Center of Cosmic Rays and Radiation Events in the Atmosphere) project.

Financial support. This research has been supported by the Ministry of Education, Youth and Science (grant no. CZ.02.1.01/0.0/0.0/15_003/0000481).

Review statement. This paper was edited by Thomas Wagner and reviewed by two anonymous referees.

References

Abbasi, R. U., Abu-Zayyad, T., Allen, M., Barcikowski, E., Belz, J. W., Bergman, D. R., Blake, S. A., Byrne, M., Cady, R., Cheon, B. G., Chiba, J., Chikawa, M., Fujii, T., Fukushima, M., Furlich, G., Goto, T., Hanlon, W., Hayashi, Y., Hayashida, N., Hibino, K., and Zundel, Z.: Gamma ray showers observed at ground level in coincidence with downward lightning leaders, J. Geophys. Res.-Atmos., 123, 6864–6879, https://doi.org/10.1029/2017JD027931, 2018.

Belz, J. W., Krehbiel, P. R., Remington, J., Stanley, M. A., Abbasi, R. U., LeVon, R., Rison, W., Rodeheffer, D., Abu-Zayyad, T., Allen, M., Barcikowski, E., Bergman, D. R., Blake, S. A., Byrne, M., Cady, R., Cheon, B. G., Chikawa, M., di Matteo, A., Fujii, T., Fujita, K., Fujiwara, R., Fukushima, M., Furlich, G., Hanlon, W., Hayashi, M., Hayashi, Y., Hayashida, N., Hibino, K., Honda, K., Ikeda, D., Inadomi, T., Inoue, N., Ishii, T., Ito, H., Ivanov, D., Iwakura, H., Jeong, H. M., Jeong, S., Jui, C. C. H., Kadota, K., Kakimoto, F., Kalashev, O., Kasahara, K., Kasami, S., Kawai, H., Kawakami, S., Kawata, K., Kido, E., Kim, H. B., Kim, J. H., Kim, J. H., Kuzmin†, V., Kuznetsov, M., Kwon, Y. J., Lee, K. H., Lubsandorzhiev, B., Lundquist, J. P., Machida, K., Matsumiya, H., Matthews, J. N., Matuyama, T., Mayta, R., Minamino, M., Mukai, K., Myers, I., Nagataki, S., Nakai, K., Nakamura, R., Nakamura, T., Nakamura, Y., Nonaka, T., Oda, H., Ogio, S., Ohnishi, M., Ohoka, H., Oku, Y., Okuda, T., Omura, Y., Ono, M., Oshima, A., Ozawa, S., Park, I. H., Potts, M., Pshirkov, M. S., Rodriguez, D. C., Rubtsov, G., Ryu, D., Sagawa, H., Sahara, R., Saito, K., Saito, Y., Sakaki, N., Sako, T., Sakurai, N., Sano, K., Seki, T., Sekino, K., Shibata, F., Shibata, T., Shimodaira, H., Shin, B. K., Shin, H. S., Smith, J. D., Sokolsky, P., Sone, N., Stokes, B. T., Stroman, T. A., Takagi, Y., Takahashi, Y., Takeda, M., Takeishi, R., Taketa, A., Takita, M., Tameda, Y., Tanaka, K., Tanaka, M., Tanoue, Y., Thomas, S. B., Thomson, G. B., Tinyakov, P., Tkachev, I., Tokuno, H., Tomida, T., Troitsky, S., Tsunesada, Y., Uchihori, Y., Udo, S., Uehama, T., Urban, F., Wallace, M., Wong, T., Yamamoto, M., Yamaoka, H., Yamazaki, K., Yashiro, K., Yosei, M., Yoshii, H., Zhezher, Y., and Zundel, Z.: Observations of the Origin of Downward Terrestrial Gamma-Ray Flashes, J. Geophys. Res.-Atmos., 125, e2019JD031940, https://doi.org/10.1029/2019JD031940, 2020.

Chilingarian, A.: Thunderstorm Ground Enhancements (TGEs) – New High-Energy Phenomenon Originated in the Terrestrial Atmosphere, J. Phys. Conf. Ser., 409, 012019, https://doi.org/10.1088/1742-6596/409/1/012019, 2013.

Chilingarian, A., Hovsepyan, G., and Hovhannisyan, A.: Particle bursts from thunderclouds: Natural particle accelerators above our heads, Phys. Rev. D, 83, 062001, https://doi.org/10.1103/PhysRevD.83.062001, 2011.

Chum, J., Langer, R., Baše, J., Kollárik, M., Strhárský, I., Diendorfer, G., and Rusz, J.: Significant enhancements of secondary cosmic rays and electric field at the high mountain peak of Lomnický Štít in High Tatras during thunderstorms, Earth Planets Space, 72, 28, https://doi.org/10.1186/s40623-020-01155-9, 2020.

Dwyer, J. R.: A fundamental limit on electric fields in air, Geophys. Res. Lett., 30, 2055, https://doi.org/10.1029/2003GL017781, 2003.

Dwyer, J. R., Schaal, M. M., Cramer, E., Arabshahi, S., Liu, N., Rassoul, H. K., Hill, J. D., Jordan, D. M., and Uman, M. A.: Observation of a gamma-ray flash at ground level in association with a cloud-to-ground lightning return stroke, J. Geophys. Res.-Space, 117, A10303, https://doi.org/10.1029/2012JA017810, 2012.

Enoto, T., Wada, Y., Furuta, Y., Nakazawa, K., Yuasa, T., Okuda, K., Makishima, K., Sato, M., Sato, Y., Nakano, T., Umemoto, D., and Tsuchiya, H.: Photonuclear reactions triggered by lightning discharge, Nature, 551, 481–484, https://doi.org/10.1038/nature24630, 2017.

Fishman, G. J., Bhat, P. N., Mallozzi, R., Horack, J. M., Koshut, T., Kouveliotou, C., Pendleton, G. N., Meegan, C. A., Wilson, R. B., Paciesas, W. S., Goodman, S. J., and Christian, H. J.: Discovery of intense gamma-ray flashes of atmospheric origin, Science, 264, 1313–1316, https://doi.org/10.1126/science.264.5163.1313, 1994.

Fujifilm: FE185 Series, Super wide-angle lenses, Fujifilm, https://www.fujifilm.com/us/en/business/optical-devices/machine-vision-lens/fe185-series (last access: 13 April 2022), 2021.

Gurevich, A. V., Milikh, G. M., and Roussel-Dupre, R.: Runaway electron mechanism of air breakdown and preconditioning during a thunderstorm, Phys. Lett. A, 165, 463–468, https://doi.org/10.1016/0375-9601(92)90348-P, 1992.

Kakona, M.: Lightning over the sky. In situ ground-based mobile measurement of lightning events above central Europe, TIB AV-Portal [video], https://doi.org/10.5446/60389, 2022a.

Kakona, M.: Positive leader side of lightning development and recoil leaders. In situ ground-based mobile measurement of lightning events above central Europe, TIB AV-Portal [video], https://doi.org/10.5446/60390, 2022b.

Kakona, M.: Negative leader side of lightning development time-lapse. In situ ground-based mobile measurement of lightning events above central Europe, TIB AV-Portal [video], https://doi.org/10.5446/60388, 2022c.

Kereszy, I., Rakov, V. A., Ding, Z., and Dwyer, J. R.: Ground-Based Observation of a TGF Occurring Between Opposite Polarity Strokes of a Bipolar Cloud-To-Ground Lightning Flash, J. Geophys. Res.-Atmos., 127, e2021JD036130, https://doi.org/10.1029/2021JD036130, 2022.

Kochkin, P., van Deursen, A. P. J., Marisaldi, M., Ursi, A., de Boer, A. I., Bardet, M., Allasia, C., Boissin, J. F., Flourens, F., and Østgaard, N.: In-Flight Observation of Gamma Ray Glows by ILDAS, J. Geophys. Res.-Atmos., 122, 12801–12811, https://doi.org/10.1002/2017JD027405, 2017.

KronTechInc.: CHRONOS 1.4 DATASHEET, KronTechInc., https://www.krontech.ca/wp-content/uploads/2021/09/FM-ENGR-50001-Chronos-1.4-Datasheet-Rev5.pdf (last access: 13 April 2022), 2021.

López, J. A., Pineda, N., Montanyà, J., Velde, O. v. d., Fabró, F., and Romero, D.: Spatio-temporal dimension of lightning flashes based on three-dimensional Lightning Mapping Array, Atmos. Res., 197, 255–264, https://doi.org/10.1016/j.atmosres.2017.06.030, 2017.

Mazur, V., Ruhnke, L. H., Warner, T. A., and Orville, R. E.: Recoil leader formation and development, J. Electrost., 71, 763–768, https://doi.org/10.1016/j.elstat.2013.05.001, 2013.

McCarthy, M. and Parks, G. K.: Further observations of X-rays inside thunderstorms, Geophys. Res. Lett., 12, 393–396, https://doi.org/10.1029/GL012i006p00393, 1985.

Michimoto, K.: Meteorological Aspects of Winter Thunderstorms along the Hokuriku Coast of Japan, IEEJ Transactions on Power and Energy, 127, 1242–1246, https://doi.org/10.1541/ieejpes.127.1242, 2007.

MLAB: Barometric sensor with termometer WINDGAUGE03A, MLAB, https://mlab.cz/module/ALTIMET01A (last access: 13 April 2022), 2015.

MLAB: VLF antenna interconnection module, GitHub, https://github.com/mlab-modules/VLFANT01 (last access: 13 April 2022), 2017.

MLAB: Venturi tube based anemometer WINDGAUGE03A, MLAB, https://www.mlab.cz/module/WINDGAUGE03A (last access: 13 April 2022), 2020.

MLAB: Electric Field mill interface module FIELDMILL01A, MLAB, https://www.mlab.cz/module/FIELDMILL01A (last access: 13 April 2022), 2021.

Østgaard, N., Neubert, T., Reglero, V., Ullaland, K., Yang, S., Genov, G., Marisaldi, M., Mezentsev, A., Kochkin, P., Lehtinen, N., Sarria, D., Qureshi, B. H., Solberg, A., Maiorana, C., Albrechtsen, K., Budtz-Jørgensen, C., Kuvvetli, I., Christiansen, F., Chanrion, O., Heumesser, M., and Al-nussirat, S.: First 10 months of TGF observations by ASIM, J. Geophys. Res.-Atmos., 124, 14024–14036, https://doi.org/10.1029/2019JD031214, 2019.

Parks, G. K., Mauk, B. H., Spiger, R., and Chin, J.: X-ray enhancements detected during thunderstorm and lightning activities, Geophys. Res. Lett., 8, 1176–1179, https://doi.org/10.1029/GL008i011p01176, 1981.

Rakov, V. A. and Kereszy, I.: Ground-based observations of lightning-related X-ray/gamma-ray emissions in Florida: Occurrence context and new insights, Electr. Pow. Syst. Res., 213, 108736, https://doi.org/10.1016/j.epsr.2022.108736, 2022.

Rakov, V. A. and Uman, M. A.: Lightning: Physics and Effects, Cambridge University Press, https://doi.org/10.1017/CBO9781107340886, 2003.

Rison, W., Thomas, R. J., Krehbiel, P. R., Hamlin, T., and Harlin, J.: A GPS-based three-dimensional lightning mapping system: Initial observations in central New Mexico, Geophys. Res. Lett., 26, 3573–3576, https://doi.org/10.1029/1999GL010856, 1999.

Shi, F., Liu, N., Dwyer, J. R., and Ihaddadene, K. M. A.: VHF and UHF Electromagnetic Radiation Produced by Streamers in Lightning, Geophys. Res. Lett., 46, 443–451, https://doi.org/10.1029/2018GL080309, 2019.

Torii, T., Takeishi, M., and Hosono, T.: Observation of gamma-ray dose increase associated with winter thunderstorm and lightning activity, J. Geophys. Res.-Atmos., 107, ACL 2-1–ACL 2-13, https://doi.org/10.1029/2001JD000938, 2002.

Tsuchiya, H., Enoto, T., Torii, T., Nakazawa, K., Yuasa, T., Torii, S., Fukuyama, T., Yamaguchi, T., Kato, H., Okano, M., Takita, M., and Makishima, K.: Observation of an energetic radiation burst from mountain-top thunderclouds, Phys. Rev. Lett., 102, 255003, https://doi.org/10.1103/PhysRevLett.102.255003, 2009.

UST: Mobile piezoelectric distrometer DISTROMETER01A, UST, https://github.com/UniversalScientificTechnologies/DISTROMETER01 (last access: 13 April 2022), 2020.

UST: UHF Radio Storm Monitoring Station, UST, https://github.com/UniversalScientificTechnologies/RSMS01 (last access: 13 April 2022), 2021.

Velychko, O., Ambrožová, I., Kákona, M., and Ploc, O.: Characterisation Of Airdos-C Detector For Measurement Of High-Energy Events In The Atmosphere, Radiat. Prot. Dosim., 198, 604–610, https://doi.org/10.1093/rpd/ncac105, 2022.

Wada, Y., Enoto, T., Nakazawa, K., Furuta, Y., Yuasa, T., Nakamura, Y., Morimoto, T., Matsumoto, T., Makishima, K., and Tsuchiya, H.: Downward Terrestrial Gamma-Ray Flash Observed in a Winter Thunderstorm, Phys. Rev. Lett., 123, 061103, https://doi.org/10.1103/PhysRevLett.123.061103, 2019.

Wanke, E.: Blitzortung.org – A low cost Time of Arrival Lightning Detection and Lightning Location Network, Universität Düsseldorf, https://www.blitzortung.org/Compendium/Documentations/Documentation_2011-04-01_Green_PCB_6.6_PCB_5.6.pdf (last access: 1 January 2023), 2011.

Windy: https://www.windy.com/ (last access: 13 April 2022), 2021.

Wu, T., Wang, D., and Takagi, N.: Lightning mapping with an array of fast antennas, Geophys. Res. Lett., 45, 3698–3705, https://doi.org/10.1002/2018GL077628, 2018.